

Origin of the DC and AC conductivity anisotropy in iron-based superconductors: scattering rate versus spectral weight effects

Michael Schütt,¹ Jörg Schmalian,² and Rafael M. Fernandes¹

¹*School of Physics and Astronomy, University of Minnesota, Minneapolis 55455, USA*

²*Institute for Theory of Condensed Matter and Institute for Solid State Physics, Karlsruhe Institute of Technology, 76128 Karlsruhe, Germany.*

To shed light on the mechanism responsible for the in-plane resistivity anisotropy in the nematic phase of the iron-based superconductors, we investigate the impact of spin fluctuations on the anisotropic AC conductivity. On the one hand, the scattering of electrons off magnetic fluctuations causes an anisotropic scattering rate. On the other hand, the accompanying Fermi velocity renormalization contributes to both the plasma frequency and the scattering rate in antagonistic ways, giving rise to anisotropies in these quantities that exactly cancel each other in the DC limit. As a result, the effective scattering rate changes its sign as function of temperature, but the DC conductivity retains the same sign, in agreement with recent experiments.

In-plane resistivity anisotropy measurements have been employed as the primary tool to investigate the nematic phase of both cuprate and iron-based superconductors [1–5]. In these systems, the onset of electronic nematic order, characterized by an Ising order parameter $\varphi \neq 0$, lowers the point-group symmetry from tetragonal to orthorhombic, making the two in-plane x and y directions inequivalent [6–8]. As a result, a non-zero conductivity anisotropy arises, $\Delta\sigma = \sigma_x - \sigma_y \neq 0$ [9].

In general, the longitudinal DC conductivity along direction $\mu = x, y$ can be expressed in terms of the Drude form $\sigma_\mu = \tau_\mu \Omega_{p,\mu}^2 / (4\pi)$, where τ_μ^{-1} is the transport scattering rate (not to be confused with the inverse single-particle lifetime) and $\Omega_{p,\mu}$ is the plasma frequency. Therefore, an anisotropy in the DC conductivity can arise from an anisotropic scattering rate, which is sensitive to impurities and to the low-energy excitations of the system, and/or from an anisotropic Drude weight, which is sensitive to the electronic structure. In the nematic phase of the iron-based superconductors, different effects contribute to these quantities. Anisotropic magnetic fluctuations triggered by nematic order [10, 11] give rise to an anisotropy in the inelastic scattering rate [12–14], whereas the dressing of an impurity potential by magnetic correlations promotes an anisotropy in the elastic scattering rate [15, 16]. Conversely, the distortion of the Fermi surface caused by the ferro-orbital order triggered at the nematic transition affect the plasma frequency [17–20]. Disentangling these contributions would provide important insight into the dominant processes responsible for the nematic instability.

At first sight, a natural way to disentangle τ_μ^{-1} and $\Omega_{p,\mu}$ is the AC conductivity, $\sigma_\mu(\omega)$. Indeed, recent measurements of $\sigma_\mu(\omega)$ in detwinned BaFe₂As₂ reported a larger anisotropy in the plasma frequency than in the scattering rate [4, 21], which was interpreted as evidence for electronic-structure induced anisotropy. However, as we show in this paper, these two quantities are unavoidably entangled. This general result follows directly from

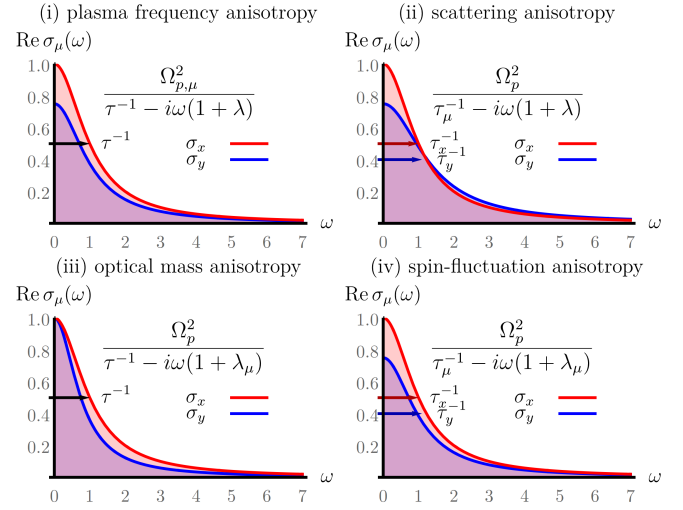


FIG. 1. AC conductivity $\sigma_\mu(\omega)$ of Eq. (1) as function of frequency ω for both x and y directions. In case (i), only the plasma frequency is anisotropic ($\Omega_{p,y}^2 = (3/4)\Omega_{p,x}^2$), while in (ii) and (iii) only the scattering rate ($\tau_y^{-1} = (4/3)\tau_x^{-1}$) and the optical mass ($\lambda_y = (4/3)\lambda_x$) are anisotropic, respectively. Panel (iv) shows the case in which both the scattering rate and the optical mass are anisotropic, yielding AC and DC conductivities very similar to those in panel (i). The causality properties of the AC conductivity do not allow cases (ii) and (iii) to exist, i.e. both τ_μ^{-1} and λ_μ must be present.

the memory function formalism, which is valid even in the absence of quasi-particles, and yields the following form for the AC conductivity [22]:

$$\sigma_\mu(\omega) = \frac{\Omega_{p,\mu}^2}{4\pi} \frac{1}{\tau_\mu^{-1}(\omega) - i\omega[1 + \lambda_\mu(\omega)]}. \quad (1)$$

The main point is that, besides $\Omega_{p,\mu}$ and τ_μ^{-1} , the AC conductivity depends additionally on the optical mass enhancement λ_μ [23]. While λ_μ does not contribute to the DC conductivity $\sigma_\mu(\omega \rightarrow 0)$, it does modify the effective plasma frequency and the effective scattering rate

extracted from a typical AC conductivity measurement, yielding $\tilde{\Omega}_{p,\mu}^2 = \Omega_{p,\mu}^2 / (1 + \lambda_\mu)$ and $\tilde{\tau}_\mu^{-1} = \tau_\mu^{-1} / (1 + \lambda_\mu)$. To illustrate the importance of this effect for the interpretation of the experimental results of Ref. [21], in Fig. 1 we plot $\text{Re}[\sigma_\mu(\omega)]$ in Eq. (1) considering four cases: (i) anisotropy only in the plasma frequency ($\Omega_{p,y} < \Omega_{p,x}$); (ii) anisotropy only in the scattering rate ($\tau_y^{-1} > \tau_x^{-1}$); (iii) anisotropy only in the optical mass ($\lambda_y > \lambda_x$); (iv) anisotropy in both scattering rate and optical mass ($\tau_y^{-1} > \tau_x^{-1}$ and $\lambda_y > \lambda_x$). The system in cases (i) and (ii) have very similar DC conductivities, but rather different AC conductivities in the intermediate frequency range. In the presence of optical mass anisotropy only, case (iii), the system does not display a DC conductivity anisotropy, but in the intermediate frequency range, the AC conductivity is similar to that of case (i). The key point is that cases (ii) and (iii) are not allowed due to the causality properties of the AC conductivity, which require *both* τ_μ^{-1} and λ_μ to be present. After combining these two effects, case (iv), the system displays DC and AC conductivities very similar to case (i). Thus, the AC conductivity anisotropy observed in Ref. [21] is in equally consistent with either case (i) or (iv), which have very different physical origins – electronic-structure anisotropy and scattering rate anisotropy, respectively.

In this paper we compute the AC conductivity of a multi-band model for the iron pnictides in which the electrons interact with spin fluctuations – which become anisotropic in the nematic phase [10, 11]. While this interaction does not promote anisotropy in the bare plasma frequency, it causes anisotropies simultaneously in both the scattering rate, $\Delta\tau^{-1} \equiv \tau_x^{-1} - \tau_y^{-1} \neq 0$, and in the optical mass, $\Delta\lambda \equiv \lambda_x - \lambda_y \neq 0$. Physically, the first effect arises from real collisions of electrons and magnetic fluctuations, whereas the latter effect stems from the reduction of the electronic Fermi velocity (or, equivalently, the enhancement of the effective electron mass) promoted by the exchange of virtual spin fluctuations (see Fig. 2).

More importantly, our microscopic calculations reveal that while the overall signs of both quantities, $\Delta\tau^{-1}$ and $\Delta\lambda$, are determined by the same prefactor that depends on the geometry of the Fermi surface [12], the relative sign of $\Delta\tau^{-1}$ and $\Delta\lambda$ is always positive, similar to case (iv) in Fig. 1. Consequently, the *effective* scattering rate anisotropy $\Delta\tilde{\tau}^{-1} = \Delta\tau^{-1} - \tau_0^{-1}\Delta\lambda$ is reduced with respect to its bare value, while the *effective* plasma frequency anisotropy $\Delta\tilde{\Omega}_p^2 = -\Omega_{p,0}^2\Delta\lambda$ is enhanced (here τ_0^{-1} and $\Omega_{p,0}$ are the bare isotropic scattering rate and plasma frequency). Interestingly, because collisions are suppressed at low temperatures, $\Delta\tau^{-1}$ decreases as the temperature is lowered. In contrast, $\Delta\lambda$ remains finite as $T \rightarrow 0$, since it is proportional to the electronic mass renormalization. Consequently, one generally expects a sign-change of $\Delta\tilde{\tau}^{-1}$ as function of temperature, despite the fact that $\Delta\sigma(\omega \rightarrow 0) \propto \Delta\tau^{-1}$ retains the same sign. These behaviors agree with recent AC conductivity mea-

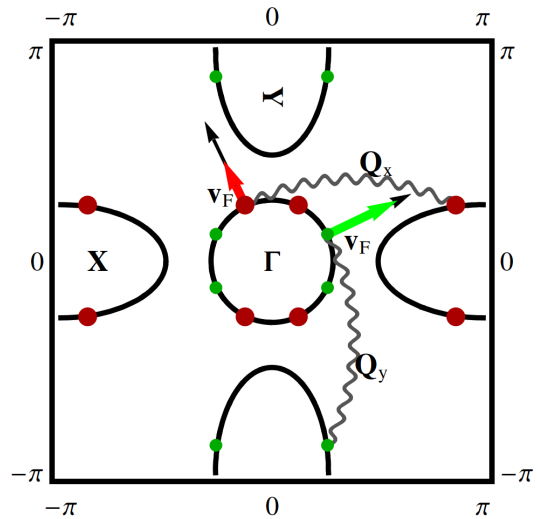


FIG. 2. Illustration of the Fermi surface, consisting of hole-like (at Γ) and electron-like pockets (at X and Y), and the anisotropic processes promoted by spin fluctuations. On the one hand, scattering off of spin fluctuations is stronger for the hot spots exchanging $\mathbf{Q}_X = (\pi, 0)$ (red dots) than $\mathbf{Q}_Y = (0, \pi)$ (green dots) fluctuations. On the other hand, the renormalized Fermi velocity suppression (or, equivalently, mass renormalization) caused by the exchange of spin fluctuations (arrows) is smaller at the red hot spots than at the green hot spots.

surements in detwinned BaFe_2As_2 [4, 21], revealing the importance of anisotropic spin fluctuations to describe the nematic state of the iron pnictides.

Our starting point is the minimal three band model shown in Fig. 2 [24], and previously employed to investigate the DC conductivity anisotropy due to the scattering by spin fluctuations [12]. This model has a hole-like circular pocket centered at the $\Gamma = (0, 0)$ point of the Fe-square lattice Brillouin zone, and two elliptical electron pockets centered at $X = (\pi, 0)$ and $Y = (0, \pi)$. Hereafter, for convenience, these bands are labeled $\beta = 0$, $\beta = 1$, and $\beta = -1$, respectively. We also include in the model point-like impurities, giving rise to the isotropic band-independent elastic scattering rate τ_0^{-1} .

To make the symmetry properties of the AC conductivity more evident, we consider the band-resolved conductivity σ_μ^β for band β in direction μ such that, $\sigma_\mu = \sum_\beta \sigma_\mu^\beta$. Without interactions, we have $\sigma_{0,\mu}^\beta = \frac{1}{4\pi} (\Omega_{p,\mu}^\beta)^2 / (\tau_0^{-1} - i\omega)$, where the subscript 0 denotes the non-interacting system and $\Omega_{p,\mu}^\beta = \sqrt{\frac{2e^2 N_F^\beta}{\hbar}} v_F^\beta$, with density of states N_F^β and averaged Fermi velocity v_F^β . The tetragonal symmetry of the system implies $\Omega_{p,x}^\beta = \Omega_{p,y}^{-\beta}$, i.e. $\sigma_{0,x}^\beta = \sigma_{0,y}^{-\beta}$, yielding $\Delta\sigma_0 \equiv \sigma_{0,x} - \sigma_{0,y} = 0$, as expected for a tetragonal system.

The contribution arising from the interaction with spin fluctuations is conveniently expressed in terms of

the memory function $M_\mu^\beta(\omega)$, defined such that $\sigma_\mu^\beta = \frac{1}{4\pi} (\Omega_{p,\mu}^\beta)^2 / [\tau_0^{-1} - i\omega + M_\mu^\beta(\omega)]$ [22]. Hence, while $\text{Re}(M_\mu^\beta)$ renormalizes the scattering rate, $-\text{Im}(M_\mu^\beta)/\omega$ renormalizes the optical mass. The fact that these two quantities are related by Kramers-Kronig relations implies that an anisotropy in the scattering rate must be accompanied by an anisotropy in the optical mass, as stated in the introduction. In this framework, calculating the band-resolved AC conductivity anisotropy, $\Delta\sigma^\beta \equiv \Delta\sigma_x^\beta - \Delta\sigma_y^\beta$, is equivalent to calculating the anisotropic memory function $\Delta M^\beta = M_x^\beta - M_y^{-\beta}$, since $\Delta\sigma^\beta = -\left(\frac{\sigma_{0,x}^\beta}{\tau_0^{-1} - i\omega}\right) \Delta M^\beta$. Consequently, expansion of ΔM^β for small frequencies yields the anisotropic scattering rate and optical mass, $\Delta M^\beta = (\Delta\tau^\beta)^{-1} - i\omega\Delta\lambda^\beta$.

To leading order in the interaction parameter g between the electrons and the spin fluctuations, the memory function is given by the two Feynman diagrams depicted in Fig. 3 [25], where solid lines denote the electronic Green's function $\mathcal{G}_k^\beta = (i\tilde{\omega}_n - \epsilon_{\mathbf{k}}^\beta)^{-1}$ and the wavy lines denote the spin fluctuation dynamic susceptibility χ_k . Here, $k = (i\omega_n, \mathbf{k})$ denotes both momentum \mathbf{k} and Matsubara frequency ω_n , $\epsilon_{\mathbf{k}}^\beta \approx \mathbf{v}_F^\beta \cdot \mathbf{k}$ is the linearized dispersion of band β , and $\tilde{\omega}_n = \omega_n + \text{sgn}(\omega_n)/(2\tau_0)$ is introduced in the Green's function to incorporate the effect of impurity scattering within the Born approximation. In particular, the memory function is given by the combination of diagrams $\left(\frac{\sigma_{0,\mu}^\beta}{\tau_0^{-1} - i\omega}\right) M_\mu^\beta = \frac{e^2}{i\omega} (2\Phi_\mu^{\text{self},\beta} + \Phi_\mu^{\text{vert},\beta})$ with:

$$\Phi_{\mu,p}^{\text{self},\beta} = g^2 \sum_{\beta'} \int_{k,k'} \chi_{k-k'}^{(\beta\beta')} \mathcal{G}_k^\beta v_{\mu,k}^\beta \mathcal{G}_{k+p}^{\beta'} \mathcal{G}_{k'+p}^{\beta'} \mathcal{G}_{k+p}^\beta v_{\mu,k+p}^\beta, \quad (2)$$

$$\Phi_{\mu,p}^{\text{vert},\beta} = g^2 \sum_{\beta'} \int_{k,k'} \chi_{k-k'}^{(\beta\beta')} \mathcal{G}_k^\beta v_{\mu,k}^\beta \mathcal{G}_{k+p}^\lambda \mathcal{G}_{k'}^{\beta'} v_{\mu,k'+p}^{\beta'} \mathcal{G}_{k'+p}^{\beta'}, \quad (3)$$

where $v_{\mu,k}^\beta$ is the velocity, $p = (i\Omega_n, 0)$, and $\int_k = T \sum_{\omega_n} \int_{\text{BZ}} d^2k / (2\pi)^2$. As shown by inelastic neutron scattering data [26], the magnetic susceptibility is peaked at the ordering vectors $\mathbf{Q}_X = (\pi, 0)$ and $\mathbf{Q}_Y = (0, \pi)$. Therefore, the only terms that contribute to the sums above are $\chi_k^{(10)} \equiv \chi_{X,k}$ and $\chi_k^{(-10)} \equiv \chi_{Y,k}$. At low energies and in the tetragonal phase, these susceptibilities are equal and described by $\chi_{j,k}^{-1} = \chi_0^{-1} (\xi^{-2} + |\mathbf{k} - \mathbf{Q}_j|^2 + |\omega_n|/\gamma)$, where χ_0^{-1} is the magnetic energy scale, ξ is the correlation length (in units of the lattice constant), and γ is the Landau damping. Indeed, this form has been widely used to fit the neutron data in pnictides [26–28]. In the nematic phase, the susceptibilities become different, since magnetic fluctuations become stronger along either \mathbf{Q}_X or \mathbf{Q}_Y . Specifically, the correlation lengths are renormalized by the nematic order

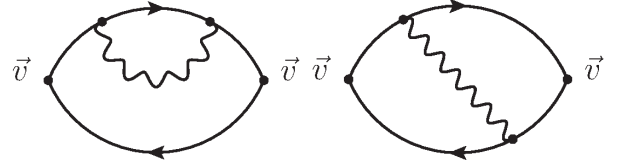


FIG. 3. Interaction corrections to the optical conductivity diagrams: self-energy Φ^{self} (left) and vertex corrections Φ^{vert} (right). Solid lines refer to the electronic propagator, wavy lines denote the spin fluctuation propagator, and \mathbf{v} is the velocity vertex.

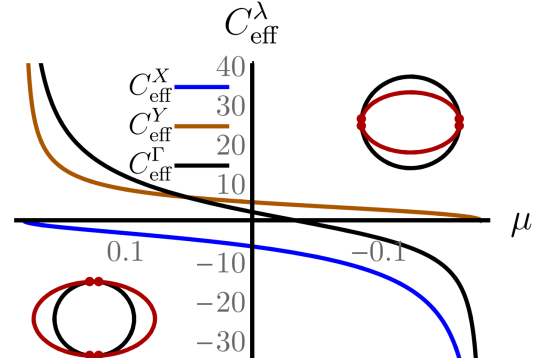


FIG. 4. The coefficient C_{eff}^β , as function of the chemical potential μ (in units of the Fermi energy ϵ_0), for a circular hole pocket at the Γ point and elliptical electron pockets centered at X and Y . The ellipticity here is set to $\delta = 0.35$.

parameter φ , yielding $\chi_{j,k}^{-1} = \chi_{j,k}^{-1} \mp \chi_0^{-1} \xi^{-2} \varphi$ [10].

Such an anisotropy in the spin fluctuation spectrum, which is indeed observed experimentally [11], is responsible for the anisotropy in the memory function. Consequently, it is useful to expand ΔM^β for small φ . In contrast to the isotropic contribution to the memory function [29], the behavior of ΔM^β is dominated by the hot spots of the Fermi surface – i.e. points of the Fermi surface connected by the magnetic ordering vectors $\mathbf{Q}_X = (\pi, 0)$ and $\mathbf{Q}_Y = (0, \pi)$, $\epsilon_{\mathbf{k}}^\beta = \epsilon_{\mathbf{k}+\mathbf{Q}_j}^{\beta'}$ (see Fig. 2). Focusing on this contribution, we find the analytical expression:

$$\Delta M^\beta(\omega) = -\varphi \tilde{g}^2 C_{\text{eff}}^\beta \omega \mathcal{K} \left(\frac{\xi^{-2} \gamma}{2\pi T}, \frac{\omega}{\xi^{-2} \gamma} \right). \quad (4)$$

where we defined the dimensionless coupling constant $\tilde{g}^2 = g^2 \chi_0 \nu_F^\beta$ and the complex function $\mathcal{K}(s, t)$:

$$\mathcal{K}(s, t) = -\frac{1}{t} \left[1 - \frac{1}{2s} + \left(1 + \frac{i}{t} \right) \times \left(\frac{1}{s} + \psi(s) - \psi(1 + s - ist) \right) \right], \quad (5)$$

with ψ denoting the digamma function. Eq. (4) naturally separates the contributions arising from the Fermi surface geometry, encoded in C_{eff}^β (see supplementary [30]

material for the full expression), and the contributions arising from the spin dynamics, encoded in $\mathcal{K}(s, t)$ via the two dimensionless parameters $s \equiv \xi^{-2}\gamma/(2\pi T)$ and $t = \omega/(\xi^{-2}\gamma)$. While s is proportional to the ratio between the spin correlation length ξ and the length scale of thermal spin fluctuations $\xi_T^2 \equiv \gamma/T$, t depends explicitly on the frequency. Because we are interested in the interaction-induced corrections to the standard Drude formula, hereafter we take the limit $t \ll 1$. Terms beyond this approximation are particularly important near quantum critical points, where $\xi \rightarrow \infty$, and at frequencies larger than the scale set by the isotropic scattering rate τ_0^{-1} , which is of the order of 300 meV in BaFe₂As₂ (see supplementary material and also [31]). Although the study of these contributions is beyond the scope of this paper, we note that for $\omega \gg \tau_0^{-1}$ they give rise to a slower decay of $\text{Re}[\sigma(\omega)]$ than the standard ω^{-2} Drude behavior [32].

In terms of the function $\mathcal{K}(s, t)$, the anisotropies in the bare scattering rate and in the optical mass are given by $(\Delta\tau^\beta)^{-1} = -\varphi\tilde{g}^2 C_{\text{eff}}^\beta \omega \text{Re}\mathcal{K}(s, t \rightarrow 0)$ and $\Delta\lambda^\beta = \varphi\tilde{g}^2 C_{\text{eff}}^\beta \text{Im}\mathcal{K}(s, 0)$, yielding the effective scattering rate and plasma frequency anisotropies:

$$\begin{aligned} (\Delta\tilde{\tau}^\beta)^{-1} &= -\varphi\tilde{g}^2 C_{\text{eff}}^\beta [\omega \text{Re}\mathcal{K}(s, t \rightarrow 0) + \tau_0^{-1} \text{Im}\mathcal{K}(s, 0)] \\ (\Delta\tilde{\Omega}_p^\beta)^2 &= -\varphi\tilde{g}^2 C_{\text{eff}}^\beta (\Omega_{p,x}^\beta)^2 \text{Im}\mathcal{K}(s, 0) \end{aligned} \quad (6)$$

As it can be confirmed by explicit evaluation of Eq. (5), the analytical properties of the complex function $\mathcal{K}(s, t)$ enforce its real part to be positive and its imaginary part to be negative. This is because the former arises from the collision of electrons by spin fluctuations – the same process that causes a finite electronic lifetime via the imaginary part of the self-energy – whereas the latter arises from the suppression of the electronic Fermi velocity – the same process that enhances the electronic mass via the real part of the self-energy (see Fig. 1). Consequently, the two contributions to $(\Delta\tilde{\tau}^\beta)^{-1}$ in Eq. (6) have opposite signs, resulting in a suppression of the effective scattering rate compared to the bare scattering rate $(\Delta\tau^\beta)^{-1}$. Furthermore, because of their different physical origins – inelastic collision *versus* Fermi velocity renormalization – the two contributions to the effective scattering rate $(\Delta\tilde{\tau}^\beta)^{-1}$ display rather different temperature dependencies. Using Eq. (5), we find that at high temperatures ($T \gg \gamma\xi^{-2}$) the behaviors $\omega \text{Re}\mathcal{K}(s, 0^+) \propto T$ and $\text{Im}\mathcal{K}(s, 0) \propto -\frac{1}{T}$, whereas at low temperatures ($T \ll \gamma\xi^{-2}$) we have $\omega \text{Re}\mathcal{K}(s, 0^+) \propto T^2$ and $\text{Im}\mathcal{K}(s, 0) = -\frac{1}{2}$. Thus, while $\text{Re}\mathcal{K} > 0$ dominates the high-temperature regime, $\text{Im}\mathcal{K} < 0$ governs the low-temperature regime. This can be physically understood from the fact that $\text{Re}\mathcal{K}$ arises from the physical collision between electrons and spin fluctuations, which are completely suppressed at $T = 0$, whereas $\text{Im}\mathcal{K}$ arises from the

suppression of the Fermi velocity, which persists down to $T = 0$.

Therefore, one expects that as temperature is lowered, the anisotropy of the effective scattering rate changes sign. Using characteristic values for BaFe₂As₂ (see supplementary material and also [31]), $\tau_0^{-1} \sim 300$ meV from the residual resistivity and $\gamma \sim 100$ meV, $\xi \sim 5a$ from neutron scattering [28], we find that the two contributions become comparable at the temperature scale $T^* \sim 100$ K. Interestingly, recent optical conductivity data in this compound [21] find such a behavior, with $(\Delta\tilde{\tau}^\beta)^{-1}$ changing sign below the nematic transition at $T_{\text{nem}} \sim 150$ K. Although these compounds display also long-range magnetic order, at these temperatures the resulting reconstruction of the Fermi surface is incipient [33], suggesting that the mechanism discussed here could be at play.

We emphasize that the sign change in the effective scattering rate $(\Delta\tilde{\tau}^\beta)^{-1}$ does not cause a sign change in the DC conductivity anisotropy – also in agreement with the experiments. Indeed, as it is clear from Eq. (1), the DC conductivity anisotropy depends only on the bare scattering rate $(\Delta\tau^\beta)^{-1}$, which in turn is solely determined by $\text{Re}\mathcal{K}$, $\Delta\sigma(\omega = 0) = -\frac{1}{4\pi} \sum_\beta (\Omega_{0,x}^\beta)^2 \tau_0^2 (\Delta\tau^\beta)^{-1}$. The main consequence of the reduction of the effective scattering rate $(\Delta\tilde{\tau}^\beta)^{-1}$ is an accompanying enhancement of the anisotropic Drude spectral weight $\Delta\text{SW} \equiv \int_0^\infty \Delta\sigma(\omega) d\omega$, since $\Delta\text{SW} = \frac{1}{8} \sum_\beta (\Delta\tilde{\Omega}_p^\beta)^2$ depends only on $\text{Im}\mathcal{K}$, as shown in Eq. (6). Physically, this means that any suppression of the effective scattering rate is compensated by an enhancement of the effective Drude weight, keeping the DC anisotropy the same.

The global sign of $\Delta\sigma(\omega = 0)$ and ΔSW depend on the same parameters C_{eff}^β via Eq. (6), which are determined by the Fermi surface geometry. We calculate them explicitly in Fig. 4 for a toy model in which the hole pocket is a circle, $\epsilon_\Gamma = \epsilon_0 - \frac{p^2}{2m}$, whereas the electron pockets are ellipses, $\epsilon_{X/Y} = \frac{p_x^2}{2m(1\pm\delta)} + \frac{p_y^2}{2m(1\mp\delta)} - \epsilon_0$ [12, 34]. By fixing the ellipticity δ , we find that in general the weighted sum of C_{eff}^β is positive for electron-doped compounds ($\mu > 0$) and negative for hole-doped compounds ($\mu < 0$). Consequently, because $\varphi > 0$ for a detwinned sample with tensile strain applied along the x direction [11], we find $\Delta\sigma > 0$ and $\Delta\text{SW} > 0$ for electron-doped compounds, and $\Delta\sigma < 0$ and $\Delta\text{SW} < 0$ for hole-doped compounds. This agrees with previous theoretical calculations using the Boltzmann equation instead of the diagrammatic approach used here [12, 14], as well as with experiments [35, 36].

In summary, we studied the impact of anisotropic spin fluctuations on the optical conductivity anisotropy of the nematic phase of iron-based superconductors. Our main result is that, in this case, while the DC conductivity

anisotropy is determined solely by the collision of electrons and spin fluctuations, the electronic Fermi velocity renormalization induced by spin fluctuations causes opposite changes in the effective scattering rate and plasma frequencies anisotropies that exactly compensate each other in the DC limit. Our results qualitatively agree with recent optical conductivity experiments in detwinned BaFe_2As_2 . Experimental optical studies of compounds that display nematic order without magnetic order, such as FeSe , would be desirable to further elucidate this unavoidable entanglement between scattering rate and plasma frequency anisotropies in these materials.

We thank fruitful discussions with J. Chu, A. Chubukov, L. Degiorgi, I. Fisher, D. Maslov, and S. Syzranov. M. S. acknowledges the support from the Humboldt Foundation. J.S. acknowledges the support from Deutsche Forschungsgemeinschaft (DFG) through the Priority Program SPP 1458 ‘‘Hochtemperatur-Supraleitung in Eisenpniktiden’’ (project-no. SCHM 1031/5-1). R. M. F. is supported by the U.S. Department of Energy, Office of Science, Basic Energy Sciences, under Award No. DE-SC0012336.

-
- [1] Y. Ando, K. Segawa, S. Komiya, and A. N. Lavrov, *Phys. Rev. Lett.* **88**, 137005 (2002).
- [2] J.-H. Chu, J. G. Analytis, K. De Greve, P. L. McMahon, Z. Islam, Y. Yamamoto, and I. R. Fisher, *Science* **329**, 824 (2010).
- [3] M. A. Tanatar, E. C. Blomberg, A. Kreyssig, M. G. Kim, N. Ni, A. Thaler, S. L. Bud’ko, P. C. Canfield, A. I. Goldman, I. I. Mazin, and R. Prozorov, *Phys. Rev. B* **81**, 184508 (2010).
- [4] A. Dusza, A. Lucarelli, A. Sanna, S. Massidda, J.-H. Chu, I. R. Fisher, and L. Degiorgi, *New Journal of Physics* **14**, 023020 (2012).
- [5] O. Cyr-Choinière, G. Grissonnanche, S. Badoux, J. Day, D. A. Bonn, W. N. Hardy, R. Liang, N. Doiron-Leyraud, and L. Taillefer, *ArXiv e-prints* (2015).
- [6] E. Fradkin, S. A. Kivelson, M. J. Lawler, J. P. Eisenstein, and A. P. Mackenzie, *Annual Review of Condensed Matter Physics* **1**, 153 (2010).
- [7] M. Vojta, *Advances in Physics* **58**, 699 (2009).
- [8] R. M. Fernandes, A. V. Chubukov, and J. Schmalian, *Nature Physics* **10**, 97 (2014).
- [9] M. Schütt and R. M. Fernandes, *Phys. Rev. Lett.* **115**, 027005 (2015).
- [10] R. M. Fernandes and J. Schmalian, *Superconductor Science and Technology* **25**, 084005 (2012).
- [11] X. Lu, J. T. Park, R. Zhang, H. Luo, A. H. Nevidomskyy, Q. Si, and P. Dai, *Science* **345**, 657 (2014).
- [12] R. M. Fernandes, E. Abrahams, and J. Schmalian, *Phys. Rev. Lett.* **107**, 217002 (2011).
- [13] S. Liang, G. Alvarez, C. Şen, A. Moreo, and E. Dagotto, *Phys. Rev. Lett.* **109**, 047001 (2012).
- [14] M. Breitkreiz, P. M. R. Brydon, and C. Timm, *Phys. Rev. B* **90**, 121104 (2014).
- [15] M. P. Allan, T.-M. Chuang, F. Massee, Y. Xie, N. Ni, S. L. Bud’ko, G. S. Boebinger, Q. Wang, D. S. Dessau, P. C. Canfield, M. S. Golden, and J. C. Davis, *Nat Phys* **9**, 220 (2013).
- [16] M. N. Gastiasoro, I. Paul, Y. Wang, P. J. Hirschfeld, and B. M. Andersen, *Phys. Rev. Lett.* **113**, 127001 (2014).
- [17] C.-C. Chen, J. Maciejko, A. P. Sorini, B. Moritz, R. R. P. Singh, and T. P. Devereaux, *Phys. Rev. B* **82**, 100504 (2010).
- [18] W. Lv and P. Phillips, *Phys. Rev. B* **84**, 174512 (2011).
- [19] B. Valenzuela, E. Bascones, and M. J. Calderón, *Phys. Rev. Lett.* **105**, 207202 (2010).
- [20] Yin Z. P., Haule K., and Kotliar G., *Nat Phys* **7**, 294 (2011).
- [21] C. Mirri, A. Dusza, S. Bastelberger, M. Chinotti, L. Degiorgi, J.-H. Chu, H.-H. Kuo, and I. R. Fisher, *Phys. Rev. Lett.* **115**, 107001 (2015).
- [22] W. Götze and P. Wölfle, *Phys. Rev. B* **6**, 1226 (1972).
- [23] D. N. Basov and T. Timusk, *Rev. Mod. Phys.* **77**, 721 (2005).
- [24] R. M. Fernandes, A. V. Chubukov, J. Knolle, I. Eremin, and J. Schmalian, *Phys. Rev. B* **85**, 024534 (2012).
- [25] S. V. Syzranov and J. Schmalian, *Phys. Rev. Lett.* **109**, 156403 (2012).
- [26] Inosov D. S., Park J. T., Bourges P., Sun D. L., Sidis Y., Schneidewind A., Hradil K., Haug D., Lin C. T., Keimer B., and Hinkov V., *Nat Phys* **6**, 178 (2010).
- [27] S. O. Diallo, D. K. Pratt, R. M. Fernandes, W. Tian, J. L. Zarestky, M. Lumsden, T. G. Perring, C. L. Broholm, N. Ni, S. L. Bud’ko, P. C. Canfield, H.-F. Li, D. Vaknin, A. Kreyssig, A. I. Goldman, and R. J. McQueeney, *Phys. Rev. B* **81**, 214407 (2010).
- [28] G. S. Tucker, R. M. Fernandes, H.-F. Li, V. Thampy, N. Ni, D. L. Abernathy, S. L. Bud’ko, P. C. Canfield, D. Vaknin, J. Schmalian, and R. J. McQueeney, *Phys. Rev. B* **86**, 024505 (2012).
- [29] A. Abanov, A. V. Chubukov, and J. Schmalian, *Advances in Physics* **52**, 119 (2003).
- [30] See Supplemental Material [url], which includes Refs.[9, 31].
- [31] D. C. Johnston, *Advances in Physics* **59**, 803 (2010).
- [32] A detailed study of the isotropic AC conductivity in this limit will be reported elsewhere.
- [33] C. Liu, A. D. Palczewski, R. S. Dhaka, T. Kondo, R. M. Fernandes, E. D. Mun, H. Hodovanets, A. N. Thaler, J. Schmalian, S. L. Bud’ko, P. C. Canfield, and A. Kaminski, *Phys. Rev. B* **84**, 020509 (2011).
- [34] I. Eremin and A. V. Chubukov, *Phys. Rev. B* **81**, 024511 (2010).
- [35] E. C. Blomberg, M. A. Tanatar, R. M. Fernandes, I. I. Mazin, B. Shen, H.-H. Wen, M. D. Johannes, J. Schmalian, and R. Prozorov, *Nat Commun* **4**, 1914 (2013).
- [36] H.-H. Kuo, J.-H. Chu, S. A. Kivelson, and I. R. Fisher, *ArXiv e-prints* (2015), arXiv:1503.00402 [cond-mat.suprcon].

I. SUPPLEMENTARY MATERIAL: “ORIGIN OF THE RESISTIVITY ANISOTROPY IN THE IRON PNICTIDES: SCATTERING RATE OR PLASMA FREQUENCY?”

A. Form of the Geometric Coefficient

The geometric coefficient C_{eff}^β appearing in Eq. (4) of the main text is determined using direction-resolved Fermi momentum $\mathbf{p}_F(\phi)$ and Fermi velocity $\mathbf{v}_F(\phi)$ [9]. Consequently this yields a direction-resolved density of states $N(\phi) = \mathbf{p}_F^2(\phi)/(2\pi\mathbf{v}_F(\phi)\mathbf{p}_F(\phi))$, and the density of states of a single band $\nu_F^\beta = \int_0^{2\pi} N^\beta(\phi)d\phi/(2\pi)$. Using this notation, we can express the direction-average of an arbitrary function $f(\phi)$ according to $\nu_F \langle f(\phi) \rangle_\phi = \int_0^{2\pi} N(\phi)f(\phi)d\phi/(2\pi)$. The angle ϕ here is always measured with respect to the x-axis in each pocket, as shown in Fig 5.

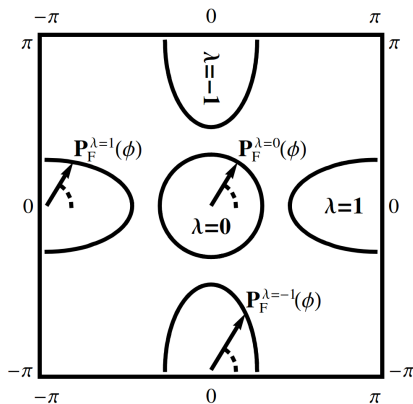


FIG. 5. Illustration of the direction resolved parametrization of the Fermi surface and the labeling of the bands involved.

Two bands that satisfy the constraint $|\beta + \beta'| = 1$ specify which of the two electron bands is interacting with the hole band in the Brillouin center. The anisotropy arises from the hot spots, the points on the Fermi surface which upon translation by either $\mathbf{Q}_X = (\pi, 0)$ or $\mathbf{Q}_Y = (0, \pi)$ connect the two involved bands, i.e. $\epsilon_{\mathbf{k}}^\beta =$

$\epsilon_{\mathbf{k}+\mathbf{Q}_j}^{\beta'}$. These hot spot are characterized by the hot spot angles $\phi_{\text{HS}(\beta\beta')}$. In terms of these quantities, the geometric coefficient is given by:

$$C_{\text{eff}}^\beta = \sum_{\substack{\beta' \\ |\beta+\beta'|=1}} (\beta + \beta') \frac{N^\beta(\phi_{\text{HS}(\beta\beta')})N^{\beta'}(\phi_{\text{HS}(\beta\beta')})}{\left| \frac{\partial \mathbf{p}_F^\beta}{\partial \phi_{\text{HS}(\beta\beta')}} \times \frac{\partial \mathbf{p}_F^{\beta'}}{\partial \phi_{\text{HS}(\beta\beta')}} \right|} \times \frac{\left[v_{x,F}^\beta(\phi_{\text{HS}(\beta\beta')}) - v_{x,F}^{\beta'}(\phi_{\text{HS}(\beta\beta')}) \right]^2}{2\pi\nu_F^\beta\nu_F^{\beta'} \langle (v_{x,F}^\beta)^2 \rangle_\phi} \quad (7)$$

For the coefficient of the hole pocket $\beta = 0$, the summation includes the other two electron bands. However since the objects above obey the C_4 symmetry of the system ($f^\beta(\phi + \pi/2) = f^{-\beta}(\phi)$ and $\mathbf{g}^\beta(\phi + \pi/2) = -i\sigma_y \mathbf{g}^{-\beta}(\phi)$ for any C_4 symmetric scalar function f or vector function \mathbf{g}), the contribution can be re-expressed in the familiar form that is proportional to $(v_x^\beta - v_x^{\beta'})^2 - (v_y^\beta - v_y^{\beta'})^2$.

B. Estimative of the impurity scattering rate

We estimated the impurity scattering rate from the residual resistivity $\rho_0 = \tau_0^2 m / (ne^2)$. For simplicity, we consider the system as a cylindrical Fermi surface, such that the density can be expressed according to $n = k_F^2 / (2\pi c)$. Consequently the scattering rate is found to be:

$$\tau_0^{-1} h = \rho_0 e^2 h k_F^2 / (2\pi m c) = \rho_0 h \bar{k}_F^2 e^2 / (mV) \quad (8)$$

where in the last step we measured the Fermi momentum in units of the inverse lattice constant a and the unit cell volume $V = a^2 c$ has been used. Using typical values for the 122 pnictides [31]: we have $\bar{k}_F \approx \pi/4$, $a = 4 \text{ \AA}$, $c = 6.5 \text{ \AA}$, $\rho_0 \approx 0.3 \text{ m}\Omega \cdot \text{cm} = 3 \times 10^{-6} \Omega \cdot \text{m}$, yielding:

$$\tau_0^{-1} h \approx 330 \text{ meV} \quad (9)$$